Editors' Suggestion

Bias-Free Access to Orbital Angular Momentum in Two-Dimensional Quantum Materials

Jonas Erhardt,[1,2] Cedric Schmitt,[1,2] Philipp Eck,[3,2] Matthias Schmitt,[1,4] Philipp Keßler,[1,2] Kyungchan Lee,[1,2] Timur Kim,[4] Cephise Cacho,[4] Iulia Cojocariu,[5,6,7] Daniel Baranowski,[6] Vitaliy Feyer,[6,8] Louis Veyrat,[1,2,9,10] Giorgio Sangiovanni,[3,2] Ralph Claessen,[1,2] and Simon Moser[1,2,*]

[1]*Physikalisches Institut, Universität Würzburg, D-97074 Würzburg, Germany*
[2]*Würzburg-Dresden Cluster of Excellence ct.qmat, Universität Würzburg, D-97074 Würzburg, Germany*
[3]*Institut für Theoretische Physik und Astrophysik, Universität Würzburg, D-97074 Würzburg, Germany*
[4]*Diamond Light Source, Harwell Science and Innovation Campus, Didcot, OX11 0DE, United Kingdom*
[5]*Elettra-Sincrotrone, S.C.p.A, Trieste, 34149, Italy*
[6]*Peter Grünberg Institute (PGI-6), Forschungszentrum Jülich GmbH, Jülich, 52428, Germany*
[7]*Dipartimento di Fisica, Università degli Studi di Trieste, via A. Valerio 2, 34127 Trieste, Italy*
[8]*Faculty of Physics and Center for Nanointegration Duisburg-Essen (CENIDE), Universität Duisburg-Essen, 47047 Duisburg, Germany*
[9]*Leibniz Institute for Solid State and Materials Research, IFW Dresden, D-01069 Dresden, Germany*
[10]*Laboratoire National des Champs Magnétiques Intenses, CNRS-INSA-UJF-UPS, UPR3228, 143 avenue de Rangueil, F-31400 Toulouse, France*

(Received 15 January 2024; revised 6 March 2024; accepted 8 April 2024; published 6 May 2024)

The demonstration of a topological band inversion constitutes the most elementary proof of a quantum spin Hall insulator (QSHI). On a fundamental level, such an inverted band gap is intrinsically related to the bulk Berry curvature, a gauge-invariant fingerprint of the wave function's quantum geometric properties in Hilbert space. Intimately tied to orbital angular momentum (OAM), the Berry curvature can be, in principle, extracted from circular dichroism in angle-resolved photoemission spectroscopy (CD-ARPES), were it not for interfering final state photoelectron emission channels that obscure the initial state OAM signature. Here, we outline a *full-experimental* strategy to avoid such interference artifacts and isolate the clean OAM from the CD-ARPES response. Bench-marking this strategy for the recently discovered atomic monolayer system indenene, we demonstrate its distinct QSHI character and establish CD-ARPES as a scalable bulk probe to experimentally classify the topology of two-dimensional quantum materials with time reversal symmetry.

DOI: 10.1103/PhysRevLett.132.196401

The topological classification of two-dimensional (2D) materials is traditionally connected to edge states [1] and the demonstration of the quantum spin Hall effect [2,3]. The topology of a material, however, is genuinely associated to a material's *bulk*, and should thus be experimentally accessible irrespective of the presence of a boundary. Berry curvature, the local manifestation of a wave function's geometric properties in momentum space, is intimately tied to topology [4,5], is gauge invariant, and, in principle, observable. More fundamental classification schemes have thus focused on bulk experiments that map the Berry curvature and/or the quantum geometric tensor in momentum space [6,7], promising a fast and scalable way of fingerprinting the vast plethora of potential topological materials predicted by theory [8].

To this end, circular dichroism in angle resolved photoemission spectroscopy (CD-ARPES) stands out as a powerful probe of Berry curvature owed to its well-established sensitivity to orbital angular momentum (OAM) along the light's quantization axis [9–13]. In a two band system and within approximations, both quantities are linearly connected [14,15] and OAM thus serves as mediator between CD-ARPES and Berry curvature [11,12,15,16]. Unfortunately, the CD-ARPES signal is generally subject to photoemission final state interference effects, which in turn depend on the photoelectron's kinetic energy (and due to energy conservation thus also on photon energy). These interferences produce artifacts that obscure the initial state OAM contribution [17,18]. In face of a generally uncharted final state, the extraction of OAM from CD-ARPES at a random photon energy therefore demands sophisticated data analysis in unison with case-specific theoretical efforts, jeopardizing the quest for a bias-free experimental probe of topology.

Here we demonstrate a two-step strategy that avoids the influence of the final state and enables a bias-free all-experimental isolation of OAM in *any* 2D quantum material with time-reversal symmetry (TRS). While two-dimensionality suppresses the out-of-plane band dispersion and thus allows us to probe a particular Bloch state

 © 2024 American Physical Society

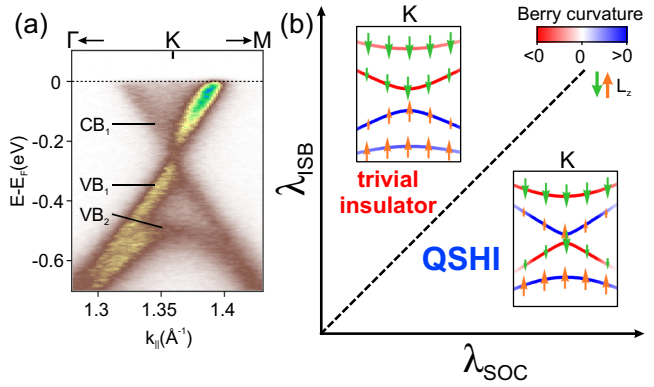

FIG. 1. (a) ARPES dispersion at the K point of n-doped indenene showing the two valence bands (VB_1, VB_2) as well as a partially occupied conduction band CB_1 ($h\nu = 21.2$ eV 20 K). (b) Topological phase diagram of a p-electron system on the triangular lattice as a function of ISB (λ_{ISB}) and SOC strength (λ_{SOC}). The insets show the $\langle L_z \rangle$ polarization (green and orange arrows) and the Berry curvature (red and blue curves) of the valence and conduction band states at K, calculated by DFT for the topologically trivial and nontrivial (QSHI) system. The topology of the system is reflected in both the OAM as well as the Berry curvature ordering sequence [19,21,22].

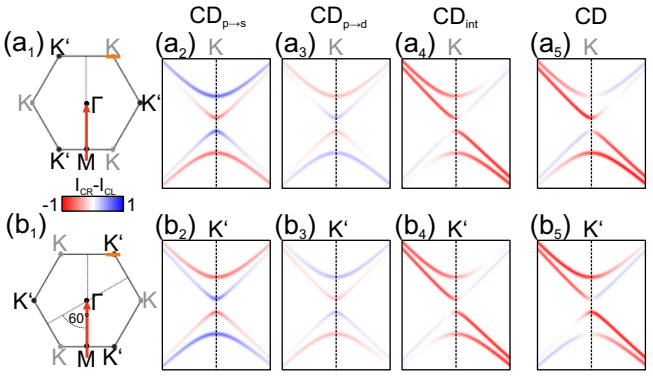

FIG. 2. Photoelectron emission channel resolved CD-ARPES calculated according to Ref. [17] for the tight-binding model derived in Refs. [19] and [21]. Panels (a) and (b) represent calculations with the light incidence plane (red arrow) along ΓM, for two experimental geometries rotated by 60° with respect to each other (a_1), (b_1). Panels (a_2), (b_2) show the s channel, (a_3), (b_3) the d channel, (a_4), (b_4) their interference channel and (a_5), (b_5) the total CD-ARPES dispersion around K and K' along the orange path in (a_1) and (b_1), respectively. Details are given in the Supplemental Material [22].

irrespective of photon energy, TRS implies the existence of time-reversal invariant momenta (TRIM) and pairs of time-reversal partners (TRP), whose (paired) OAM is strictly zero by symmetry. Nonzero CD-ARPES intensity at TRIMs or pairs of TRP is thus a clear indicator of final state artifacts. In the first step (i), we hence exploit the tunable photon energies of a synchrotron light source and the imaging capabilities of a k-space microscope to identify those $h\nu$, where the CD-ARPES signal vanishes according to TRS. At these photon energies we then analyze in step (ii) the angular distribution of CD-ARPES with respect to the orbital symmetry of the final state, and eliminate accidental false zeros obtained in step (i). We are left with a set of *faithful* photon energies where CD-ARPES isolates the pure OAM polarization signal along the light quantization axis.

We test this experimental strategy to confirm the QSHI state of the 2D quantum material indenene, a Dirac-system realized on a triangular lattice [Fig. 1(a)] whose topology is dictated by the competition of atomic spin-orbit coupling (SOC) and substrate-mediated in-plane inversion symmetry breaking (ISB) at the TRPs K and K' [19,20]. Density functional theory (DFT) predicts SOC to drive the topological band inversion and to stagger both $\langle L_z \rangle$ OAM as well as Berry curvature along the energy axis [19,21], while ISB counteracts SOC and favors a topologically trivial band order as summarized in the topological phase diagram of Fig. 1(b). Determining the $\langle L_z \rangle$ order of indenene and placing it within this diagram is an exquisite task for CD-ARPES and its potency to unambiguously determine the $\langle L_z \rangle$ sequence in the presence of TRS.

Before turning to the actual experiments, we recapitulate how artifacts masking initial state OAM can arise from CD-ARPES. Without loss of generality, we illustrate our arguments for the indenene case, whose valley states are well described by band representations built from atomic p orbitals [19,21]. Photoemission from these states will produce two dipole-allowed transition channels, from p to s (s channel), and from p to d (d channel), whose amplitudes and phases are dictated by the elusive photoelectron final state. The interference of both channels amounts to the total CD-ARPES intensity [22]

$$\mathrm{CD} = \mathrm{I}_{\circlearrowleft} - \mathrm{I}_{\circlearrowright} = \mathrm{CD}_{\mathrm{p}\to\mathrm{s}} + \mathrm{CD}_{\mathrm{p}\to\mathrm{d}} + \mathrm{CD}_{\mathrm{int}}(\Delta\sigma) \qquad (1)$$

that consists of three terms: the pure channel terms $\mathrm{CD}_{\mathrm{p}\to\mathrm{s}}$ and $\mathrm{CD}_{\mathrm{p}\to\mathrm{d}}$ that provide the clean OAM information; and the mixed channel interference term $\mathrm{CD}_{\mathrm{int}}(\Delta\sigma)$ that strongly depends on the photon energy dependent phase $\Delta\sigma$ between outgoing photoelectron waves.

Following our formalism introduced in Ref. [17], we now model the CD-ARPES intensity expected for a tight-binding model of indenene in the topological phase [21]. We take the 65° light incidence geometry along the ΓM plane that we use later in experiment [vertical red arrow in Fig. 2(a_1)], providing a contrast ratio $\langle L_z \rangle / \langle L_\parallel \rangle = |\cot 65°|^2 \sim 0.2$ of out-of-plane to in-plane OAM components [22]. Assuming—for sake of illustration—equal magnitudes of s and d channels and an extreme phase delay $\Delta\sigma = \pi/2$ between them, we simulate CD-ARPES along the perpendicular $K'MK$ direction that we employ later in experiment, and plot a close-up around K in Fig. 2.

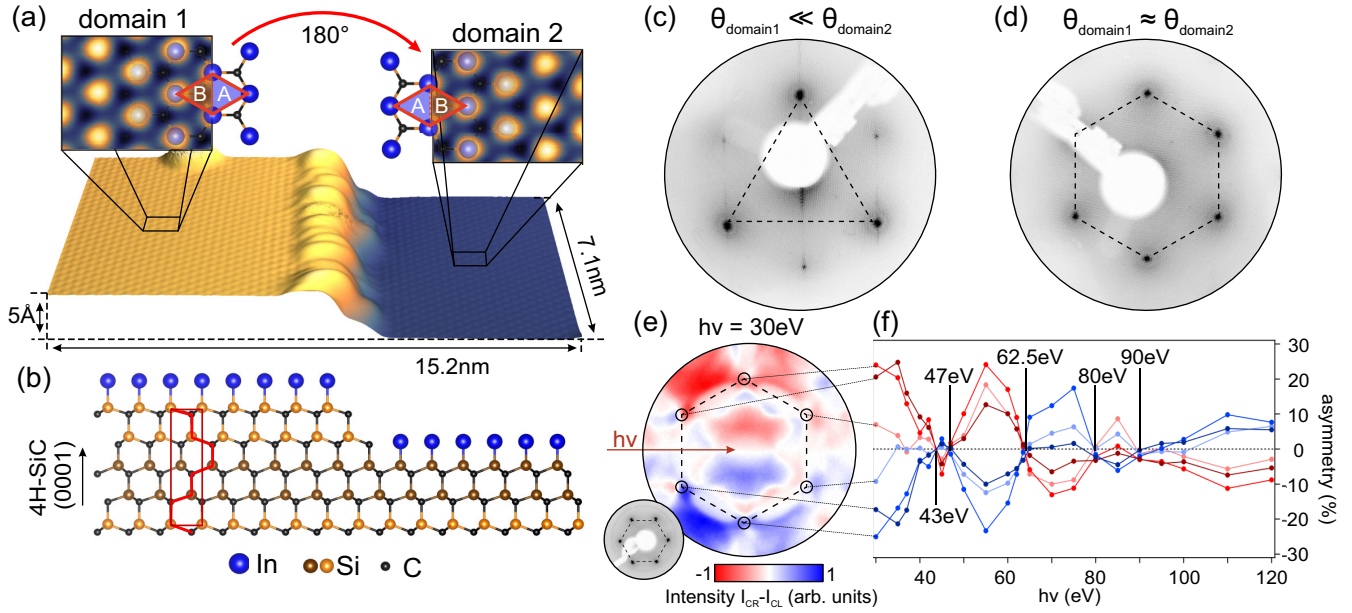

FIG. 3. Step (i)—Identification of potentially faithful photon energies: (a) 3D visualization of an STM topography scan (bias voltage: 750 mV, tunneling current: 150 pA) across a half (≈5 Å) 4H-SiC unit cell step edge, exposing two indenene domains (insets) that are mutually rotated by 180° (which in C_3 symmetry corresponds to a 60° rotation and flips K and K'). (b) Side view ball and stick model of the step structure depicted in (a), emphasizing a 180° rotation in the 4H-SiC stacking order at every half unit cell (red path). LEED pattern of (c) single domain indenene and (d) a two domain indenene sample taken at 135 eV. (e) CD-ARPES map of the two-domain sample taken at $h\nu = 30$ eV and 65° light incidence (red arrow) along the $M\Gamma M$ direction of the hexagonal BZ (dashed) and energy-integrated over the indenene valence bands range. The inset shows the LEED pattern of this sample. (f) CD-ARPES integrated around the six valley momenta [circles in (e)] and plotted as a function of photon energy. Collective zeros in the CD-signal mark photon energies where the photoemission channel interference is potentially suppressed. These energies are candidates for faithful photon energies in step (ii).

Taken by themselves, the s (a_2) and d channels (a_3) correctly map the $\langle L_z \rangle$ staggering apart from a sign change. The latter reflects that photoemission from an $m_l = \pm 1$ initial state can reach the photoelectron s channel ($m_l = 0$) only via right (left) circular polarization ($m_{\circlearrowright/\circlearrowleft} = \mp 1$), while the d channel contains $m_l = \pm 2$ and thus can also be reached by left (right) circular polarized light ($m_{\circlearrowleft/\circlearrowright} = \pm 1$). In contrast to the pure channels, the interference part in Fig. 2(a_4) deviates strongly from the alternating pattern, as it mostly reflects the photon energy dependent phase shift $\Delta\sigma(h\nu)$ between s and d channels that produces the well-known left-right asymmetry of CD-ARPES with respect to the light incidence plane [22]. Our model clearly demonstrates that this asymmetry dominates the total CD-ARPES signal (a_5), thus masking the intrinsic OAM.

That such a geometric contribution carries indeed no OAM information can be further demonstrated by exploiting TRS, which demands the $\langle L_z \rangle$ OAM polarization of the TRPs K and K' to differ only in sign. We thus simulate a 60° azimuthal rotation that exchanges K with K' but leaves the experimental geometry otherwise untouched [Fig. 2(b_1)]. While again, the pure s- and d-channel contributions to CD-ARPES correctly reproduce the sign change in the $\langle L_z \rangle$ pattern [Fig. 2(b_2, b_3)], neither CD_{int} nor the total CD are significantly affected by the 60° turn (b_4, b_5). We hence conclude that a faithful extraction of OAM from CD-ARPES requires the interference term to be suppressed, i.e., either the amplitude of s or d channel to be zero [17,22].

We identify such suppression points by measuring the CD-ARPES signal across a wide range of photon energies $h\nu$, while monitoring high symmetry points in the Brillouin zone (BZ) for which TRS dictates zero orbital polarization. In indenene, we monitor the total CD-ARPES summed over both time reversal partners K and K', a quantity that can be conveniently extracted for samples grown on a stepped SiC substrate. As shown by scanning tunneling microscopy (STM) in Fig. 3(a), such substrates support the formation of two indenene domains that are mutually rotated by 180° (which in C_3 symmetry corresponds to a 60° rotation that swaps K and K'), thus superposing K and K' in the ensemble average. The side-view model of Fig. 3(b) shows the 4H-SiC(0001) stacking order and its truncation by full (left) and half (right) unit cells at the surface. The positions of the topmost carbon atoms cause the 180° rotation between the two resulting surface configurations, producing two indenene domains whose inequivalent Wyckoff sites A and B are swapped across a half unit cell step edge [$c/2 \sim 5$ Å, Fig. 3(a)] [23]. Employing step bunching during the

initial substrate preparation phase [24–27], we can tune the substrate termination ratio and consequently the coverage ratio of the two indenene domains. In particular, we produced samples with a single indenene domain as indicated by the threefold low energy electron diffraction (LEED) pattern in Fig. 3(c) [28], as well as samples with close to 1:1 domain ratio and a sixfold LEED pattern as shown in Fig. 3(d) [22,28]. For the latter, CD-ARPES at the valley momenta now measures a signal superposition from both time reversal partners K and K', whose total OAM should strictly cancel. A detection of nonzero CD-ARPES at these points thus signals final state interference artifacts.

Figure 3(e) shows an exemplary CD-ARPES map measured for a sample with 1:1 domain ratio and $h\nu = 30$ eV at the NanoESCA momentum microscope of Elettra synchrotron, Trieste [29]. The map covers an entire BZ of indenene (dashed lines) and exhibits a typical signal asymmetry with respect to the plane of light incidence expected from geometric dichroism [39]. Repeating this measurement for a dense grid of photon energies up to 120 eV and integrating the CD-ARPES signal around the six encircled valley momenta, we obtain their respective $h\nu$ dependencies plotted in Fig. 3(f). Except for five distinct points (43, 47, 62.5, 80, and 90 eV), we observe finite CD-ARPES signal over the entire photon energy range and conclude that for the most part, i.e., for an arbitrary $h\nu$, CD-ARPES is *not* a faithful probe of OAM. In contrast, the zeros in Fig. 3(f) correctly map the suppression of total OAM at the valley momenta of the two domain system, and thus mark photon energies where the OAM of indenene can potentially be isolated.

We thus proceed to step (ii) of our strategy, and measure high resolution CD-ARPES at beam line I05 of the Diamond Light Source, Didcot [30,40]. The CD-ARPES energy dispersions along the $K'MK$ line are summarized for different sample rotations and photon energies in Fig. 4. Figure 4(a) shows results of a single-domain sample and thus clearly distinguishable K and K' momenta measured at $h\nu = 80$ eV. We detect a strong dichroism sequence at K that inverts at K' and thus reflects the OAM characteristics expected for indenene in the QSHI phase [cf. Fig. 1(c)]. Upon a 60° sample rotation in Fig. 4(b), exchanging K and K', we observe that the valley dichroism gets inverted, demonstrating its intrinsic nature. Following our arguments above, CD-ARPES at $h\nu = 80$ eV is thus a faithful representation of indenene's intrinsic OAM [41].

While the CD-ARPES systematics at $h\nu = 80$ eV in Figs. 4(a) and 4(b) is qualitatively also reproduced for 90 eV, and can be extended to further sample rotations by 120° and 180° [22], we observe a global sign change of the dichroism signal at 47 eV, as seen in Fig. 4(c). As this sign change marks a switch of dipole transition from an $m_l = 0$ to an $m_l = \pm 2$ final state, we conclude that the photoemission s channel must be suppressed for at least one of the faithful photon energies.

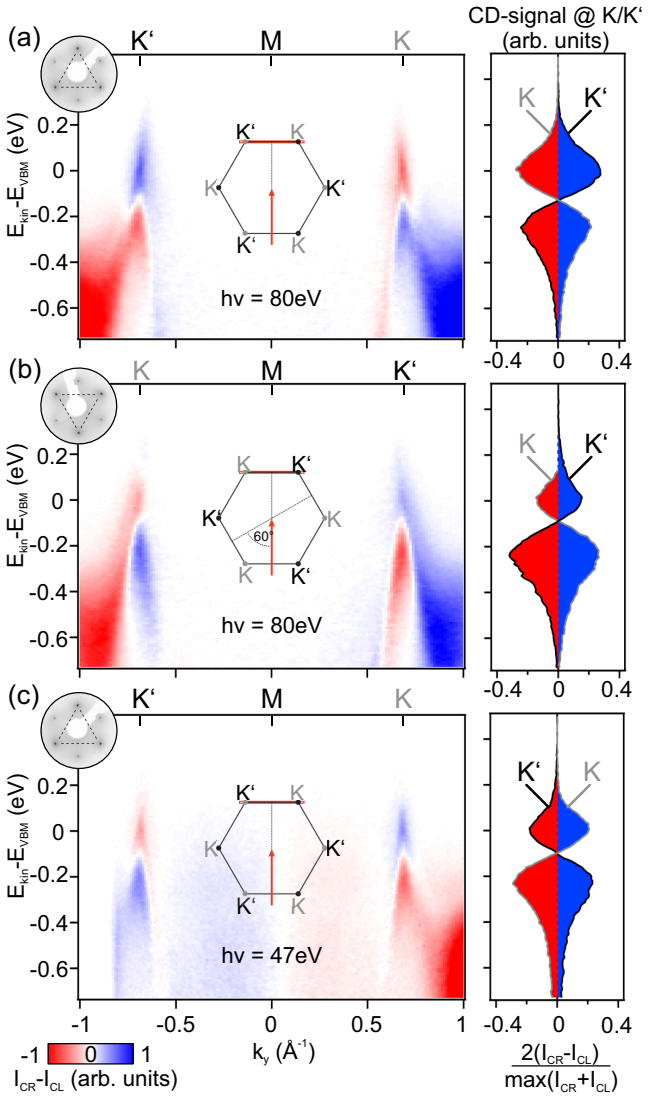

FIG. 4. Step (ii)—Confirmation and characterization of faithful photon energies: High resolution CD-ARPES measurements of a single domain indenene sample for $h\nu = 80$ (a),(b) and 47 eV (c). Shown are the CD-ARPES disperion (left) as well as dichroic energy distribution curves at the valley momenta (right). The light incidence plane with respect to the hexagonal BZ of indenene is sketched in the inset. Rotation of the sample by 60° in (b) swaps TRP K and K' and, consequently, inverts the dichroism signal. (c) CD-ARPES at a different faithful photon energy flips the sign of CD-ARPES as consequence of a switch of final states from $m_l = 0$ to $m_l = \pm 2$. Inset: LEED images taken at 135 eV indicate the single domain phase.

For completeness, we also measured the CD-ARPES dispersion of the single domain sample at $h\nu = 62.5$ eV, but found the dichroism asymmetry at K/K' to reproduce the interference artifact CD_{int} discussed above [22], marking this energy as unfaithful for OAM extraction. We further examined the CD-ARPES of the sample with 1:1 domain ratio at $h\nu = 80$ eV and found the valley dichroism to be strongly suppressed. Similarly, we studied the single

domain sample at unfaithful photon energies, but found the valley dichroism to remain invariant under 180° rotation [22]—both cross-checks that support the reliability of our strategy.

In this context, we also note that the $h\nu = 80$ eV CD-ARPES signal in Figs. 4(a) and 4(b) located far away from the valley momenta at around $\sim \pm 1$ Å^{-1} is not affected by the rotation, even though the energy is faithful. In contrast to the pure $\langle L_z \rangle$ polarization observed at K and K', this indicates a finite in-plane $\langle L_\parallel \rangle$ OAM due to admixture of p_z-orbital character to these states. The observed CD asymmetry is thus intrinsic, reflecting the rotation invariant tangential component of this in-plane OAM as predicted by DFT (see Fig. 8 in Ref. [21]).

Finally, we wish to emphasize that our OAM isolation strategy only requires knowledge about the translation group of the investigated 2D system, i.e., knowledge about its crystal system that is readily obtained from LEED or ARPES, but does *not* depend on any *a priori* information on its explicit layer group and associated point group symmetries. It thus constitutes a *bias-free*, *all-experimental* probe of OAM polarization along the light quantization axis. In combination with spin-resolution, this method establishes a fast screening method for the topology of QSHI candidates [15] as well as other 2D quantum materials such as kagome metals [16] or transition metal dichalcogenides [42]. It can be easily extended to linear dichroism in ARPES that—in combination with CD-ARPES—allows for a full reconstruction of the initial state wave function [17], hence bypassing the need to approximate Berry curvature by OAM in the first place.

We thank Domenico Di Sante for seminal contributions to the understanding of indenene's topology at the earliest stages of this project. We are grateful for funding support from the Deutsche Forschungsgemeinschaft (DFG, German Research Foundation) under Germany's Excellence Strategy through the Würzburg-Dresden Cluster of Excellence on Complexity and Topology in Quantum Matter ct.qmat (EXC 2147, Project ID 390858490) as well as through the Collaborative Research Center SFB 1170 ToCoTronics (Project ID 258499086). We acknowledge Diamond Light Source for time at beamline I05 (proposal SI30583-1) and Elettra-Sincrotrone Trieste for time at NanoESCA (proposal 20205032). We gratefully acknowledge the Gauss Centre for Supercomputing e.V. for funding this project by providing computing time on the GCS Supercomputer SuperMUC-NG at Leibniz Supercomputing Centre. L. V. was supported by the Leibniz Association through the Leibniz Competition.

*simon.moser@uni-wuerzburg.de

[1] F. Reis, G. Li, L. Dudy, M. Bauernfeind, S. Glass, W. Hanke, R. Thomale, J. Schäfer, and R. Claessen, Science **357**, 287 (2017).

[2] M. König, S. Wiedmann, C. Brüne, A. Roth, H. Buhmann, L. W. Molenkamp, X.-L. Qi, and S.-C. Zhang, Science **318**, 766 (2007).

[3] I. Knez, R.-R. Du, and G. Sullivan, Phys. Rev. Lett. **107**, 136603 (2011).

[4] M. Z. Hasan and C. L. Kane, Rev. Mod. Phys. **82**, 3045 (2010).

[5] X.-L. Qi and S.-C. Zhang, Rev. Mod. Phys. **83**, 1057 (2011).

[6] N. Fläschner, B. S. Rem, M. Tarnowski, D. Vogel, D.-S. Lühmann, K. Sengstock, and C. Weitenberg, Science **352**, 1091 (2016).

[7] A. Gianfrate, O. Bleu, L. Dominici, V. Ardizzone, M. De Giorgi, D. Ballarini, G. Lerario, K. W. West, L. N. Pfeiffer, D. D. Solnyshkov, D. Sanvitto, and G. Malpuech, Nature (London) **578**, 381 (2020).

[8] B. Bradlyn, L. Elcoro, J. Cano, M. G. Vergniory, Z. Wang, C. Felser, M. I. Aroyo, and B. A. Bernevig, Nature (London) **547**, 298 (2017).

[9] S. R. Park, J. Han, C. Kim, Y. Y. Koh, C. Kim, H. Lee, H. J. Choi, J. H. Han, K. D. Lee, N. J. Hur, M. Arita, K. Shimada, H. Namatame, and M. Taniguchi, Phys. Rev. Lett. **108**, 046805 (2012).

[10] M. Ünzelmann, H. Bentmann, P. Eck, T. Kißlinger, B. Geldiyev, J. Rieger, S. Moser, R. C. Vidal, K. Kißner, L. Hammer, M. A. Schneider, T. Fauster, G. Sangiovanni, D. Di Sante, and F. Reinert, Phys. Rev. Lett. **124**, 176401 (2020).

[11] S. Cho, J.-H. Park, J. Hong, J. Jung, B. S. Kim, G. Han, W. Kyung, Y. Kim, S.-K. Mo, J. D. Denlinger, J. H. Shim, J. H. Han, C. Kim, and S. R. Park, Phys. Rev. Lett. **121**, 186401 (2018).

[12] S. Cho, J.-H. Park, S. Huh, J. Hong, W. Kyung, B.-G. Park, J. D. Denlinger, J. H. Shim, C. Kim, and S. R. Park, Sci. Rep. **11**, 1684 (2021).

[13] M. Ünzelmann, H. Bentmann, T. Figgemeier, P. Eck, J. N. Neu, B. Geldiyev, F. Diekmann, S. Rohlf, J. Buck, M. Hoesch, M. Kalläne, K. Rossnagel, R. Thomale, T. Siegrist, G. Sangiovanni, D. D. Sante, and F. Reinert, Nat. Commun. **12**, 3650 (2021).

[14] D. Xiao, M.-C. Chang, and Q. Niu, Rev. Mod. Phys. **82**, 1959 (2010).

[15] M. Schüler, U. D. Giovannini, H. Hübener, A. Rubio, M. A. Sentef, and P. Werner, Sci. Adv. **6**, eaay2730 (2020).

[16] D. Di Sante, C. Bigi, P. Eck, S. Enzner, A. Consiglio, G. Pokharel, P. Carrara, P. Orgiani, V. Polewczyk, J. Fujii, P. D. C. King, I. Vobornik, G. Rossi, I. Zeljkovic, S. D. Wilson, R. Thomale, G. Sangiovanni, G. Panaccione, and F. Mazzola, Nat. Phys. **19**, 1135 (2023).

[17] S. Moser, J. Electron Spectrosc. Relat. Phenom. **262**, 147278 (2023).

[18] C. S. Kern, A. Haags, L. Egger, X. Yang, H. Kirschner, S. Wolff, T. Seyller, A. Gottwald, M. Richter, U. De Giovannini, A. Rubio, M. G. Ramsey, F. C. Bocquet, S. Soubatch, F. S. Tautz, P. Puschnig, and S. Moser, Phys. Rev. Res. **5**, 033075 (2023).

[19] M. Bauernfeind, J. Erhardt, P. Eck, P. Thakur, J. Gabel, T.-L. Lee, J. Schäfer, S. Moser, D. D. Sante, R. Claessen, and G. Sangiovanni, Nat. Commun. **12**, 5396 (2021).

[20] J. Erhardt, M. Bauernfeind, P. Eck, M. Kamp, J. Gabel, T.-L. Lee, G. Sangiovanni, S. Moser, and R. Claessen, J. Phys. Chem. C **126**, 16289 (2022).
[21] P. Eck, C. Ortix, A. Consiglio, J. Erhardt, M. Bauernfeind, S. Moser, R. Claessen, D. Di Sante, and G. Sangiovanni, Phys. Rev. B **106**, 195143 (2022).
[22] See Supplemental Material at http://link.aps.org/supplemental/10.1103/PhysRevLett.132.196401, which includes Refs. [17,19–21,23–38], for additional experimental information and a detailed discussion of the theoretical calculations.
[23] M. Stockmeier, R. Müller, S. A. Sakwe, P. J. Wellmann, and A. Magerl, J. Appl. Phys. **105**, 033511 (2009).
[24] V. Borovikov and A. Zangwill, Phys. Rev. B **79**, 245413 (2009).
[25] S. Nie, C. Lee, R. Feenstra, Y. Ke, R. Devaty, W. Choyke, C. Inoki, T. Kuan, and G. Gu, Surf. Sci. **602**, 2936 (2008).
[26] A. Nakajima, H. Yokoya, Y. Furukawa, and H. Yonezu, J. Appl. Phys. **97**, 104919 (2005).
[27] V. Ramachandran, M. F. Brady, A. R. Smith, R. M. Feenstra, and D. W. Greve, J. Electron. Mater. **27**, 308 (1998).
[28] D. Momeni Pakdehi, P. Schädlich, T. T. N. Nguyen, A. A. Zakharov, S. Wundrack, E. Najafidehaghani, F. Speck, K. Pierz, T. Seyller, C. Tegenkamp, and H. W. Schumacher, Adv. Funct. Mater. **30**, 2004695 (2020).
[29] C. Schneider, C. Wiemann, M. Patt, V. Feyer, L. Plucinski, I. Krug, M. Escher, N. Weber, M. Merkel, O. Renault, and N. Barrett, J. Electron Spectrosc. Relat. Phenom. **185**, 330 (2012).
[30] M. Hoesch, T. K. Kim, P. Dudin, H. Wang, S. Scott, P. Harris, S. Patel, M. Matthews, D. Hawkins, S. G. Alcock, T. Richter, J. J. Mudd, M. Basham, L. Pratt, P. Leicester, E. C. Longhi, A. Tamai, and F. Baumberger, Rev. Sci. Instrum. **88**, 013106 (2017).
[31] S. Glass, F. Reis, M. Bauernfeind, J. Aulbach, M. R. Scholz, F. Adler, L. Dudy, G. Li, R. Claessen, and J. Schäfer, J. Phys. Chem. C **120**, 10361 (2016).
[32] G. Kresse and J. Furthmüller, Phys. Rev. B **54**, 11169 (1996).
[33] A. V. Krukau, O. A. Vydrov, A. F. Izmaylov, and G. E. Scuseria, J. Chem. Phys. **125**, 224106 (2006).
[34] G. Kresse and D. Joubert, Phys. Rev. B **59**, 1758 (1999).
[35] P. E. Blöchl, Phys. Rev. B **50**, 17953 (1994).
[36] S. Steiner, S. Khmelevskyi, M. Marsmann, and G. Kresse, Phys. Rev. B **93**, 224425 (2016).
[37] A. A. Mostofi, J. R. Yates, Y.-S. Lee, I. Souza, D. Vanderbilt, and N. Marzari, Comput. Phys. Commun. **178**, 685 (2008).
[38] J. C. Slater and G. F. Koster, Phys. Rev. **94**, 1498 (1954).
[39] S. Moser, J. Electron Spectrosc. Relat. Phenom. **214**, 29 (2017).
[40] Here the light incidence angle is now close to 35° and the contrast ratio $\langle L_z\rangle/\langle L_\parallel\rangle = |\cot 35°|^2 \sim 2$ increases by a factor of 10 with respect to experiments at Elettra.
[41] M. Schüler, T. Pincelli, S. Dong, T. P. Devereaux, M. Wolf, L. Rettig, R. Ernstorfer, and S. Beaulieu, Phys. Rev. X **12**, 011019 (2022).
[42] S. Manzeli, D. Ovchinnikov, D. Pasquier, O. V. Yazyev, and A. Kis, Nat. Rev. Mater. **2**, 17033 (2017).